Capillary Evaporation in pores

R Roth†‡and K M Kroll†‡

† Max-Planck Institut für Metallforschung, Heisenbergstraße 3, D-70589 Stuttgart, Germany
‡ Institut für Theoretische und Angewandte Physik, Universität Stuttgart, Pfaffenwaldring 57,D-70569 Stuttgart, Germany

E-mail: Roland.Roth@mf.mpg.de

Abstract.

1. Introduction

2. Capillary Evaporation in Simple Geometries

We consider a square-well fluid in the grand canonical ensemble and describe its structure and thermodynamic properties within the framework of density-functional theory (DFT). The inter-particle interaction potential is given by

$$V_{sw}(r) = \begin{cases} \infty & , r < 2R_{HS}, \\ -\varepsilon & , 2R_{HS} \leq r < 2R_{sw}, \\ 0 & , \text{otherwise}, \end{cases} \tag{1}$$

where R_{HS} and R_{sw} is the hard-sphere and the square-well radius, respectively, and ε is the well depth. The functional $\Omega[\rho(\mathbf{r})]$ takes the form

$$\Omega[\rho(\mathbf{r})] = \mathcal{F}_{id}[\rho(\mathbf{r})] + \mathcal{F}_{ex}[\rho(\mathbf{r})] + \int d^3r\, \rho(\mathbf{r})\left(V_{ext}(\mathbf{r}) - \mu\right), \tag{2}$$

with an exactly know ideal gas contribution to the intrinsic Helmholtz free energy functional $\mathcal{F}_{id}$ and an approximate excess (over the ideal gas) free energy functional $\mathcal{F}_{ex}$. $V_{ext}(\mathbf{r})$ denotes the external and μ the chemical potential of the fluid. $\mathcal{F}_{ex}$ can be split into a hard-sphere reference part, for which we employ the White Bear version [3] of fundamental measure theory [1], and a square-well part

$$\mathcal{F}_{ex}^{sw}[\rho(\mathbf{r})] = \frac{1}{2}\int d^3r' \int d^3r''\rho(\mathbf{r}')\rho(\mathbf{r}'')V_{attr}(|\mathbf{r}' - \mathbf{r}''|), \tag{3}$$

with a simple mean-field approximation for the inter-particle attraction $V_{attr}(r)$, which is $-\varepsilon$ for $r < 2R_{sw}$ and zero otherwise.

First we recall the fluid bulk phase behavior of the square-well fluid. To this end we assume that the density profile $\rho(\mathbf{r})$ reduces to the constant bulk density ρ. From the bulk grand potential we calculate the pressure $p(\rho) = -\Omega_{bulk}/V$, where V is the volume, and the chemical potential $\mu(\rho) = \partial f/\partial\rho$ with the free energy density f. Two fluid phases, denoted

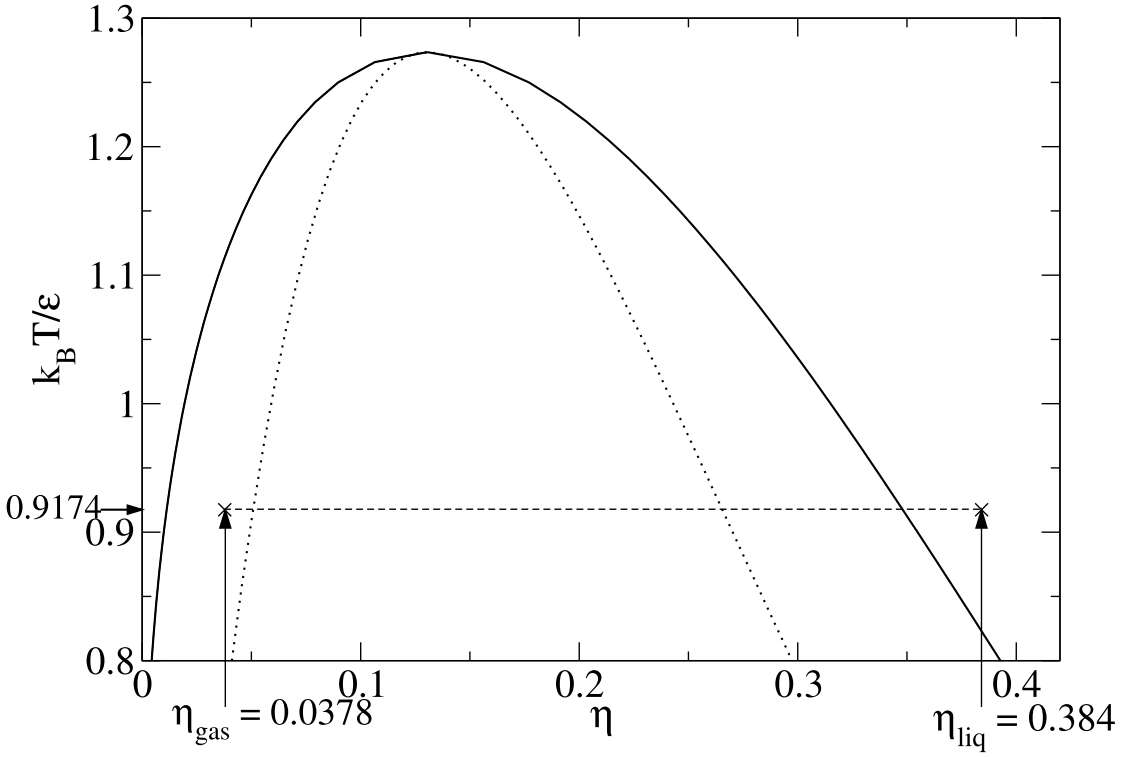

Figure 1. The fluid-gas binodal of a square-well fluid with $\sigma_{sw} = 3\sigma_{HS}$ as function of reduced temperature k_BT/ε and the fluid packing fraction $\eta = \pi\sigma_{HS}^3\,\rho/6$. In the confined geometry we consider the reduced temperature $k_BT/\varepsilon = 0.9174$ and a fluid packing fraction of $\eta_{liq} = 0.3842$. We find that a gas with $\eta_{gas} = 0.0378$ has the same chemical potential as the corresponding liquid.

by I and II, with corresponding densities ρ_I and ρ_{II} coexist when they are in mechanical and chemical equilibrium, i.e. if

$$p(\rho_I) = p(\rho_{II}), \quad \text{and} \quad \mu(\rho_I) = \mu(\rho_{II}). \tag{4}$$

For a square-well depth $R_{sw} = 3R_{HS}$ we obtain the fluid phase diagram shown in Fig. 1. Below the critical temperature, the fluid phase separates into a liquid at high density and a gas phase at low densities. Note that the mean-field perturbation theory, Eq. (3), predicts a phase diagram that is not sensitive to the detailed choice of parameters ε and R_{sw}. It rather predicts phase diagrams that can be rescaled onto a 'master phase diagram'. One finds, using the White Bear version of FMT for the hard-sphere contribution, that the critical point is located at $\eta_c \approx 0.1304$ and $k_BT_c/\varepsilon \approx 0.3773(R_{sw}/R_{HS})^3$. (**check the value**)

If we bring a square-well liquid in contact with a single purely repulsive planar wall, the fluid develops an inhomogeneous density profile $\rho(z)$, which can be calculated by minimizing the DFT with an appropriate external wall potential. For a liquid state very close to the coexisting density $\rho_{II}(T)$ one can observe complete drying and a growth of a macroscopically thick gas film at the wall as $\rho \to \rho_{II}(T)$ or the deviation $\delta\mu = \mu - \mu_{co}(T)$ from the chemical potential at coexistence $\mu_{co}(T)$ approaches zero.

In the present study, however, we shall stay away from these state points, as indicated in the phase digram in Fig. 1 by the state with reduced temperature $k_BT/\varepsilon = 0.9174$ and

packing fraction $\eta = \pi\sigma_{HS}^3\,\rho/6 = 0.3842$.

In order to quantify the change in the grand potential due to the inhomogeneous structure close to the wall we define σ the planar wall surface tension

$$\sigma = \frac{1}{A}\left(\Omega[\rho(\mathbf{r})] + pV\right), \tag{5}$$

by subtracting the bulk term $-pV$ from the total grand potential of the system $\Omega = \Omega[\rho(\mathbf{r})]$. Note that the value of σ depends on the definition of the dividing surface which in turn defines the volume V. However, the value of Ω remains well defined as long as it is calculated consistently to the dividing surface and volume.

For a state point significantly far away from the binodal, as chosen in the present case, the interaction of the liquid and a single hydrophobic wall is not sufficient to destabilize the high density liquid compared to a low density gas, because the pressure in the liquid phase away from coexistence is always higher than in a gas phase at the same chemical potential, so that the surface contribution to the grand potential can not compete with the volume term. For the gas phase to be more stable than the liquid phase, its grand potential $\Omega_g = -p_g V + \sigma_g A$ must be smaller than the grand potential of the liquid phase $\Omega_l = -p_l V + \sigma_l A$, with $V = AL$ and $L \to \infty$ in the thermodynamic limit. This can not be accomplished since even the smallest difference in the pressure would make the difference of the volume terms, $(-p_l + p_g)L$, arbitrarily larger than the difference in the surface terms, $\sigma_g - \sigma_l$.

Now we add a second, parallel, wall at distance L which we consider to have the same properties as the fist one. Note, that the value of L again depends on the definition of the dividing surface, i.e. it measures the distance between the parallel dividing surfaces of the opposing walls. If L is large compared to the correlation length ξ in the bulk liquid the grand potential of the system in the slit geometry can be written as

$$\Omega_i \approx -p_i V + 2\sigma_i A, \quad i = l, g, \tag{6}$$

where we have assumed that the walls are independent and the surface tensions σ_i are those obtained at a single wall. Since now the volume term, corresponding to a volume $V = AL$ with a finite value of L, is not scaled by an infinite length L, it is possible that the liquid phase is destabilized in a slit geometry for sufficiently small plate separations. For phase equilibrium between a liquid and a gas phase with densities ρ_l and ρ_g, respectively, it is necessary that their grand potentials and their chemical potentials equal, which can be expressed, after dividing the grand potentials by the area A, by

$$-p_l L_{CE} + 2\sigma_l = -p_g L_{CE} + 2\sigma_g, \quad \text{and} \quad \mu(\rho_l) = \mu(\rho_g). \tag{7}$$

This equilibrium condition can be solved for the slit width

$$L_{CE} = \frac{2(\sigma_g - \sigma_l)}{p_g - p_l}, \tag{8}$$

at which the capillary evaporation (CE) transition takes place. Clearly, since $(p_g - p_l)$ is negative, Eq. (8) has a physical solution only if $(\sigma_g - \sigma_l)$ as well is negative, which holds true for hydrophobic walls.

For a slit width $L > L_{CE}$ the volume term in the grand potential dominates and stabilizes the liquid phase, whereas for $L < L_{CE}$ the surface term in the grand potential becomes more

important and favors the gas phase. Note, that a gas phase that is stabilized in the slit pore, which has the same chemical potential as the liquid phase, would be meta-stable in the bulk, i.e. would lie in between the binodal (full line) and spinodal (dotted line) at $\eta_{gas} = 0.0378$.

Before we switch to a more complicated geometry it is very instructive to consider the phenomena of capillary evaporation in an infinitely long cylindrical pore. While the (approximate) form of the grand potential in the slit pore, Eq. (6), is well known and tested against microscopical theories, the case of a cylindrical pore seems less understood. Following the morphometric approach, we propose that the grand potential in contact with a complexly shaped wall can be written as

$$\Omega_i \approx -p_i V + \sigma_i A + \kappa_i C + \bar{\kappa}_i X, \tag{9}$$

where V and A are, as before, the volume and surface area defined by the dividing interface. The corresponding thermodynamical coefficients are $-p_i$ and σ_i, the negative of the pressure and the *planar* wall surface tension in phase i. Two additional geometrical measures are required in order to take the effects of curvature into account, namely C and X the integrated (over the surface area) mean and Gaussian curvatures. The corresponding thermodynamic coefficients are the bending regities κ_i and $\bar{\kappa}_i$. This form of the grand potential was suggested to describe the thermodynamics of a fluid in contact with *convex* walls, however away from a critical point or a wetting or drying transition the morphometric form of the grand potential, Eq. (9), should provide a good description also for a fluid inside of a pore, if the size of the pore is sufficiently large compared to the correlation length ξ.

For an infinitely long cylinder with radius R, the geometrical measures are readily calculated and we obtain $V = R^2\pi L$, $A = 2\pi RL$ and $C = -\pi L$. The fourth measure X vanishes because the Gaussian curvature of a cylinder is always zero. $L \to \infty$ is the length of the cylinder. Using these geometrical measures we can formulate the formulate the equilibrium condition inside of an infinite cylindrical pore

$$-p_l R_{CE}^2 + 2\sigma_l R_{CE} - \kappa_l = -p_g R_{CE}^2 + 2\sigma_g R_{CE} - \kappa_g, \quad \text{and} \quad \mu(\rho_l) = \mu(\rho_g), \tag{10}$$

where we have divided the grand potentials by πL. The radius R_{CE} at which capillary evaporation takes place can be expressed explicitly in terms of the thermodynamic coefficients as

$$R_{CE} = \frac{(\sigma_g - \sigma_l) - \sqrt{((p_g - p_l)\ (\kappa_l - \kappa_g)) + (\sigma_g - \sigma_l)^2}}{p_g - p_l}. \tag{11}$$

In order to verify the validity of the morphometric approach for the description of capillary evaporation inside of infinitely cylindrical pores, we perform DFT calculations. To this end we have to choose an external potential $V_{ext}(r)$ that defines the cylindrical pore. Since we wish to connect to the gating process in ion channels, we employ the approach from Ref. [7] and use a hard-sphere fluid of a given high density ($\eta_w = 0.4$, $R_w = 0.825 R_{HS}$) which is kept outside of the pore region by a hard-wall potential. The square-wall fluid inside the pore can hardly penetrate into the region which is occupied by the 'wall fluid'. The 'wall fluid' thereby exerts effectively an external potential $V_{ext}(r)$ on the fluid inside the pore. We have calculated the external potential $V_{ext}(r)$ so that it leads to the same density profile of the

square-well fluid inside the pore as the wall fluid does. $V_{ext}(r)$ therefore corresponds to an atomically rough hydrophobic protein wall.

We perform a series of DFT calculation of a square-well fluid inside of an cylindrical pore with radius R_{cyl}. We fix the packing fraction of the fluid $\eta = 0.3842$ and the reduced temperature $k_BT/\varepsilon = 0.9174$. The fluid density corresponds to a concentration of 55.5M, the concentration of water at normal condition, if we assume that the hard-sphere radius $R_{HS} = 1.4$Å. This state point is considerably far from the binodal, that one can expect that a capillary evaporation transition, if it happens at all, will take place at rather small values of R_{cyl}/R_{HS}.

In Fig. 2 we show the equilibrium density profiles $\rho(r)$ for varying values of R_{cyl}. For $R_{cyl} \geq 6R_{HS}$ we find that the liquid phase is stable in the cylindrical pore. In that case we observe a high density of the square-well fluid in the center of the pore and a continuous decrease to zero of the density close to the wall $r \to R_{cyl}$. For $R_{cyl} \leq 5R_{HS}$, the liquid phase inside the pore is not stable and we find a gas phase at a low density. The gas packing fraction, which is indicated in the phase diagram in Fig. 1, is $\eta_{gas} = 0.0378$ and follows from the equilibrium condition that the gas phase with this density has the same chemical potential as the high density liquid.

In order to ensure that capillary condensation takes place and to locate the radius R_{CE} at which it takes place, we also determine $\Omega[\rho(r)]/L$ the grand potential (per unit length) corresponding to the density profiles. We show the result is in Fig. 3. There are several interesting features to appreciate. Obviously, there are two separate branches of the grand potential: one corresponding to the liquid phase for large values of R_{cyl} and one corresponding to the gas phase for small values of R_{cyl}. This, together with density profiles shown in Fig. 2 demonstrates that a capillary evaporation transition happens – it is not sufficient to look solely at the profiles. The full and dashed line in Fig. 3 are fits to the grand potentials of the liquid and gas branch, respectively, according to the morphometric form Eq. (9) with the geometrical measures of the cylindrical pore. These fits are in excellent agreement with the numerical values of the grand potential obtained from DFT calculations for several values of R_{cyl}. The high quality of the fit demonstrate that the morphometric form of Ω can be employed, despite the fact that the pore is rather narrow. This finding allows the conclusion that for the problem considered here, one can separate the thermodynamic coefficients from the geometry of the pore, i.e. it is possible to extract the thermodynamic coefficients p_i, σ_i and κ_i, $i = l, g$, from the coefficients of the fits to the grand potentials on the liquid and gas branches. The pressures p_i, $i = l, g$, are bulk properties and therefore can also be determined from the bulk equation of state.

The thermodynamic coefficients obtained for our system are summarized in Tab. 1. Using these coefficients and the prediction for the radius R_{CE}, Eq. (11), at which the capillary evaporation takes place we obtain $R_{CE} = 5....R_{HS}$, which is in good agreement with the actual transition point.

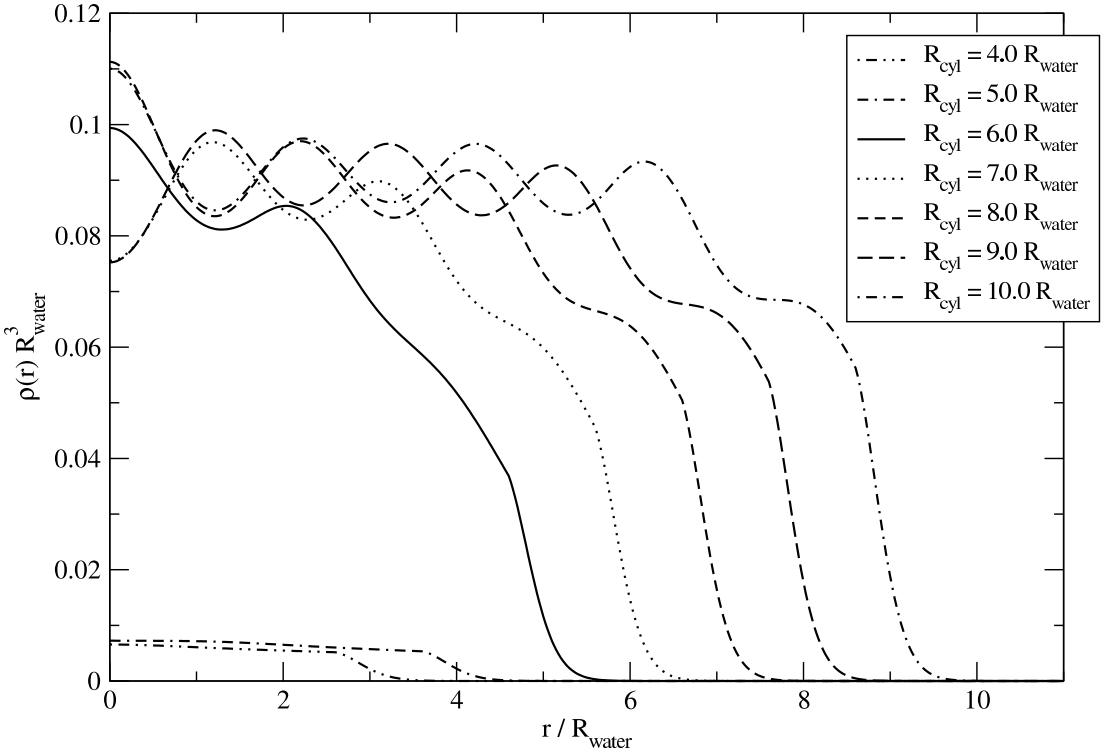

Figure 2. Density profiles $\rho(r)$ of a square well fluid inside of a cylindrical pore with hydrophobic wall-particle interaction as a function of the radius R_{cyl}. For radii $R_{cyl} \geq 6R_{HS}$ we find a liquid in the pore, while for $R_{cyl} \leq 5R_{HS}$ we find a gas. Note, however, that due to hysteresis effects it is not possible to determine the location of the capillary evaporation transition from the density profiles alone.

Table 1. Thermodynamic coefficients p_i, σ_i and κ_i, $i = l, g$ obtained for a liquid and a gas inside a cylindrical pore from a fit to DFT results, assuming a morphometric form for the grand potential.

	liquid	gas
η_i	0.3842	0.0378
$\beta p_i R_{HS}^3$	6.077×10^{-2}	5.507×10^{-3}
$\beta \sigma_i R_{HS}^2$	2.066×10^{-1}	5.816×10^{-3}
$\beta \kappa_i R_{HS}$	4.929×10^{-1}	7.708×10^{-3}

3. Capillary Evaporation in Complex Geometries

For simple geometries, like a slit pore, or an infinitely long cylindrical pore it is straightforward to perform DFT calculations in order to study the capillary evaporation phenomenon. It is also most instructive to study the thermodynamics and the density profiles at the same time. For more complex geometries a 'brute-force' approach, in which density profiles are obtained by minimizing the DFT for the full geometry, is much more challenging. We therefore will use in the following only the morphometric approach to study the analog of capillary evaporation in a complex geometry. The geometrical model, we wish to study

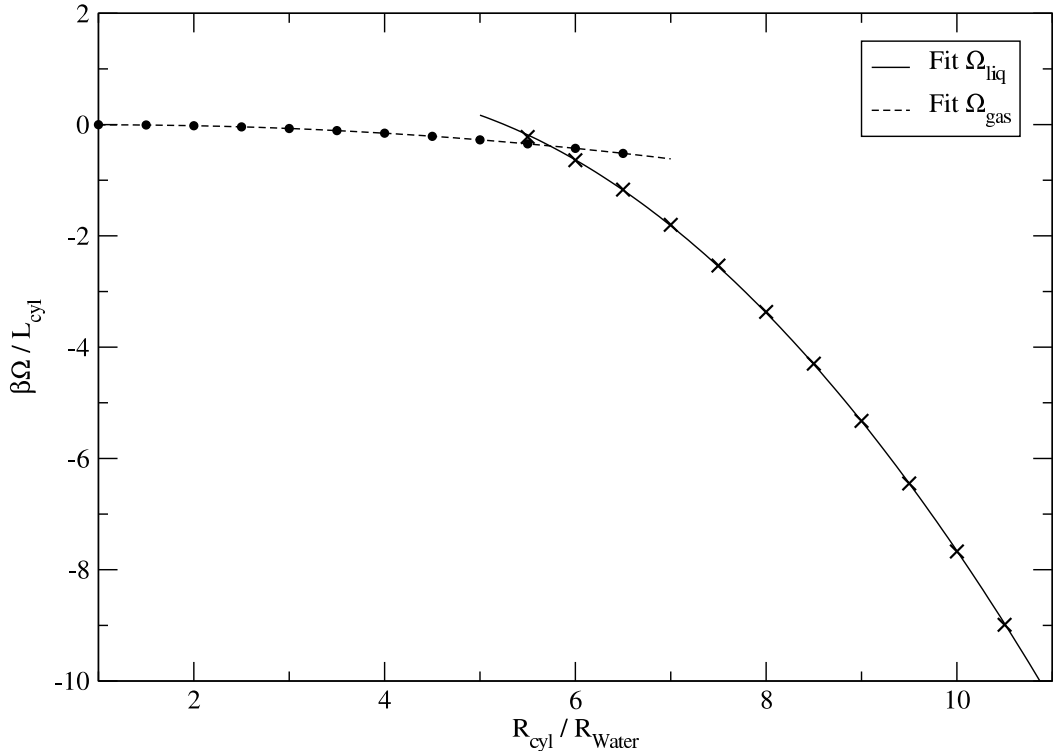

Figure 3. The grand potential per unit length of a square-well fluid inside of an infinitely long cylindrical pore as function of the radius R_{cyl}. For large values of R_{cyl} we find the liquid branch of the grand potential. Symbols correspond to DFT results and the full and dashed lines denote fits according to the morphometric form of a fluid inside of a cylindrical pore. The agreement between the morphometric form and the numerical data is excellent, indicating the validity of morphometry in this situation.

is inspired by the gating mechanism of the voltage-gated potassium ion channels, which are known to change its conformation between an open state with a wide pore in the gate region and a closed state with a somewhat narrower gate region. We show the simplified model geometry of the gate in Fig. 4, which we approximate by a part of a cone. The parameters that prescribe the geometry are the radii R_1 and R_2 and the height H. In our model R_1 and H are kept fixed and R_2 varies from a value large enough to prevent a gas bubble to block the gate, to a value small enough to allow for a closed gate with a gas bubble of height h – see Fig. 4. We consider at both end of the cone (or gate) to be big reservoirs of liquid, which will prevent the bubble to grow to macroscopic sizes. The bottom part of the gate connects to a spherical cavity of the potassium channel, while the top part of the gate connects to the outside (**check**) of the cell. Due to the geometrical constraints, the bubble, if it forms, will always have a finite size and a finite number of liquid particles will be involved in the evaporation process. Hence, the formation of a bubble represents a pseudo phase transition. In contrast to the capillary evaporation process in the infinitely long cylinder, which was either completely filled by the liquid or by the gas, we will observe two liquid-gas interfaces at the top and bottom ends of the bubble.

In the following we consider the gate with a given configuration, i.e. with a given radius

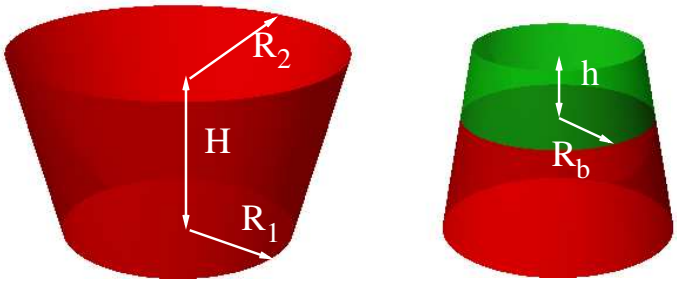

Figure 4. The model geometry of the gate of a potassium ion channel. The radius R_1 and the height H are fixed and the radius R_2 is allowed to vary from a large value, when the gate is open, to a smaller one, when the gate is closed. In the open state, the whole gate is filled with liquid, while in the closed state, a gas bubble of height h closes the gate and thereby stops the permeation of ions through the channel. R_b is the radius of the bubble at the bottom side of the bubble. Note that in the closed state there are two liquid-gas interfaces at the top and bottom of the bubble.

R_2, in a state in which it is entirely filled with the liquid and in a state with a bubble. By comparing these two states we examine the possibility of a bubble formation in the gate and study the behavior of the bubble, once it has formed. We employ the morphometric form of the grand potential for both a filled gate, which we denote as open state, and a gate with a gas bubble, which we denote as a closed state. The grand potential of the open state is given by

$$\Omega^{op}_{gate}(R_2) = -p_l\, V(H, R_1, R_2) + \sigma_l\, M(H, R_1, R_2) + \kappa_l\, C(H, R_1, R_2), \quad (12)$$

with the thermodynamical coefficients p_l, σ_l and κ_l as specified in Tab. 1. The geometrical measures for a part of a cone with height $\tilde{h}$ and radii r_1 and r_2 are given by the volume

$$V(\tilde{h}, r_1, r_2) = \frac{\pi\tilde{h}}{3}\left(r_1^2 + r_2^2 + r_1 r_2\right), \quad (13)$$

the surface area of the cone shell(**check if there is a better term**)

$$M(\tilde{h}, r_1, r_2) = \pi(r_1 + r_2)\sqrt{\tilde{h}^2 + (r_1 - r_2)^2}, \quad (14)$$

and the integrate (over the cone shell area) mean curvatures

$$C(\tilde{h}, r_1, r_2) = -\pi\tilde{h}. \quad (15)$$

Like in the case of an infinitely long cylinder, the integrated (over the cone shell area) Gaussian curvature vanishes in the cone geometry, so that the grand potential of the liquid filled gate in the morphometric form, Eq. (12) is fully specified by three terms. The morphometric form of a closed state of the gate, with a bubble of height h is more complicated and contains terms for the part of the gate filled by the liquid, terms for the part filled by the gas and terms for the liquid-gas interface contributions. It can be written as

$$\begin{aligned}\Omega^{cl}_{gate}(h, R_2) = &-p_l\, V(H-h, R_1, R_b) + \sigma_l\, M(H-h, R_1, R_b) + \kappa_l\, C(H-h, R_1, R_b)\\ &-p_g\, V(h, R_b, R_2) + \sigma_g\, M(h, R_b, R_2) + \kappa_g\, C(h, R_b, R_2)\\ &+\sigma_{lg}\,\left(A(R_b) + A(R_2)\right). \end{aligned} \quad (16)$$

Note that additional line-tension terms arise where the liquid-gas interface meets the wall. However, these contributions are expected to be small and should change the results, discussed below, only slightly. Therefore we neglect the line tension terms in the following. In order to fully specify the grand potential, Eq. (16), we require an additional thermodynamic coefficients namely σ_{lg}, the liquid-gas interface tension. Unfortunately, this quantity is rather difficult to calculate since we have to consider the interface between a liquid at high density and a gas phase, which is stabilized only in the confined geometry. This could only be done in a brute-force application of DFT in which the density profile is minimizes in the full geometry, which we wish to avoid. Therefore we approximate the value of σ_{lg} by the liquid-gas surface tension of the free interface between unconfined coexisting liquid and gas phases at the same temperature. This quantity can be calculated easily and we obtain $\beta\sigma_{lg}R_{sw}^2 = 8.549 \times 10^{-2}$. The surface area of the liquid-gas interface also calls for attention, since the radii R_1, R_2 and R_b are measured at the dividing interface. The meaning of these radii become apparent, when the density profiles in Fig. 2 are studied carefully. For a radius of the cylindrical pore $R_{cyl} = 10R_{HS}$, the liquid density profile drops to a vanishing density at $r \lesssim 9R_{HS}$. Therefore we use

$$A(r) = \pi(r - R_{HS})^2 \tag{17}$$

as the surface area of the liquid gas interface.

The first question to be addressed is the most probable bubble height h. This can be phrased as a minimization problem by asking for which value of h is the difference in the grand potential between a closed and a open state of the gate maximal, i.e.

$$\frac{\partial}{\partial h}\left(\Omega_{gate}^{cl}(h, R_2) - \Omega_{gate}^{op}(R_2)\right)\Big|_{h=h_0} = 0. \tag{18}$$

This equation can be solved explicitly. The result for h_0, however, is quite lengthy and we therefore only show numerical results for it. With this result we can answer the question for which value of R_2 the stable state of the gate is the closed one. We denote the maximal value of R_2 for which a closed gate is stable with R_2^{max}, which is defined through

$$\Delta\Omega \equiv \Omega_{gate}^{cl}(h, R_2^{max}) - \Omega_{gate}^{op}(R_2^{max}) = 0, \tag{19}$$

which can be calculated numerically.

In order to evaluate the results, we have to specify the geometry of the considered gate. We choose $R_1 = 6.43R_{HS}$ and $H = 12.86R_{HS}$, which corresponds to $R_1 \approx 9$Å and $H \approx 18$Å if we assign R_{HS} a value of 1.4Å as would be appropriate for water. For this choice of parameters, we plot in Fig. 5 the most probable height $h_0(R_2)$ as a function of the parameter R_2. For large values of R_2 we find that $h_0(R_2)$ corresponds to a meta-stable bubble, which we indicate by the dotted line. In this regime, the most stable state of the gate is the open state. As R_2 reaches the value of R_2^{max}, the bubble height jumps to a finite value and if R_2 is further decreased the bubble height increases slightly, as shown by the full line in Fig. 5. For the present model we find that the pseudo transition, at which a bubble forms in the gate, takes place for $R_2^{max} \approx 3.24R_{HS} \approx 4.53$Å , as follows from the difference in grand potential of a closed and open state of the gate with as function of R_2 – see Fig. 6.

The finite height $h_0(R_2^{max})$ can be readily understood. When we compare the grand potentials for the closed gate to that of the open gate, by calculating $\Delta\Omega$ we find

$$\Delta\Omega = -\Delta pV(h, R_b, R_2) + \Delta\sigma M(h, R_b, R_2) + \Delta\kappa C(h, R_b, R_2) \\ +\sigma_{lg}\left(A(R_b) + A(R_2)\right), \tag{20}$$

where we have introduced $\Delta p = p_l - g_g$, $\Delta\sigma = \sigma_l - \sigma_g$ and $\Delta\kappa = \kappa_l - \kappa_g$. In order to have the gate closed we require $\Delta\Omega < 0$, which we can analyze be comparing the different contributions to $\Delta\Omega$. For the situation we consider here, we find that three terms in Eq. (20) are positive, namely $\Delta pV(h, R_b, R_2) > 0$, describing the fact that the volume term prefers the stable bulk phase, i.e. the liquid, in the gate, $\Delta\kappa C(h, R_b, R_2) > 0$ and $\sigma_{lg}(A(R_b) + A(R_2)) > 0$, which simple states the fact that the formation of two liquid-gas interfaces costs energy. These three contributions to $\Delta\Omega$ have to be balanced by the only negative term $\Delta\sigma M < 0$. However, this balance can only be established if the surface area of the cone shell M is sufficiently large, which requires a finite height $h_0(R_2^{max})$.

Within this model of the gate, it is easy to estimate the energy required to control the state of the gate. If the gate is in the open state then ion permeation should not be interrupted too often due to fluctuations. This means that the value of R_2 in the open state has to be large enough that $\Delta\Omega$ stabilizes the open gate. However, if R_2 is too large in the open state, which would cause the gate to be constantly open, the energy cost to close the gate would be too high. Similar arguments can be employed for the closed state. The closed state should be stabilized against fluctuations, without too high energy costs. For our parameters, we can realize this situation if we assume that for the open state $R_2^{op} \approx R_2^{max} + 1.07R_{HS} \approx R_2^{max} + 1.5\text{Å}$ and $R_2^{cl} \approx R_2^{max} - 1.42R_{HS} \approx R_2^{max} - 2\text{Å}$. In that case the energy required to control the gate is roughly $5k_BT$, which is comparable to the electrostatic energy gain of the voltage sensor of the potassium channel.

4. Conclusion

References

[1] Rosenfeld Y 1989 Phys. Rev. Lett. ...
[2] König P M, Roth R, and Mecke K R 2004 Phys. Rev. Lett. **93** 160601
[3] Roth R, Evans R, Lang A, and Kahl G 2002 J. Phys.:Condens. Matter **14** 12063
[4] Yu Y-X and Wu J 2002 J. Chem. Phys. **117** 10156
[5] see, e.g. Evans R 1992 in *Fundamentals of Inhomogeneous Fluids* (New York: Dekker) p 85
[6] Mansoori G A, Carnahan N F, Starling K E, and Leland Jr. T W 1971 J. Chem. Phys. **54** 1523
[7] Roth R and Gillespie D 2005 Phys. Rev. Lett. **95** 247801.

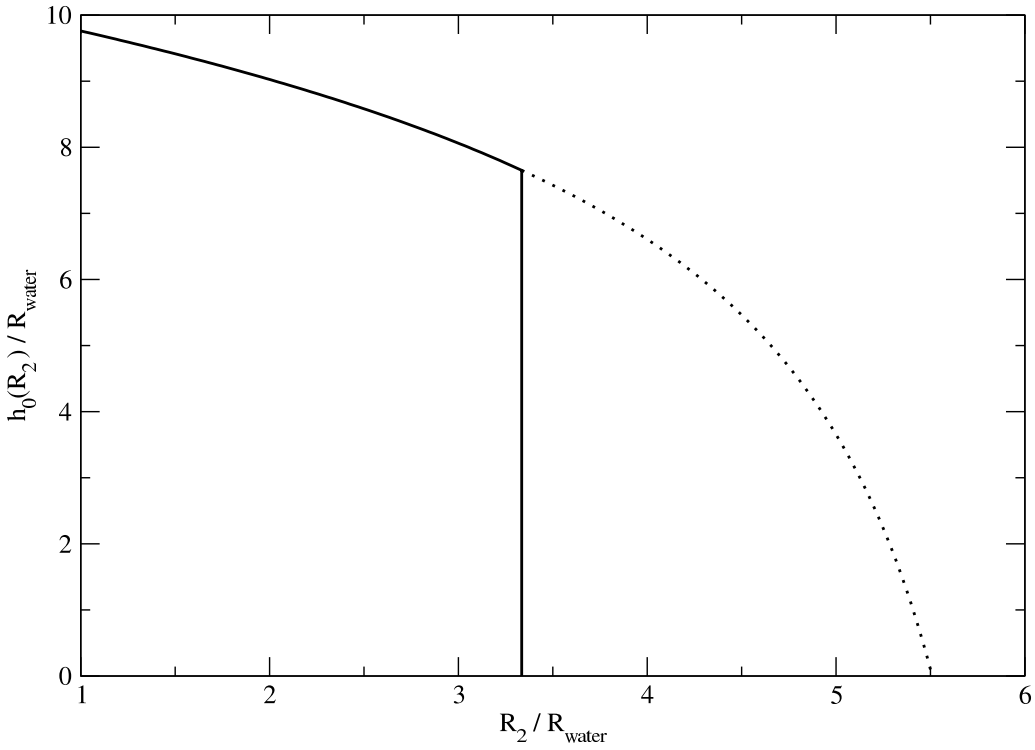

Figure 5.

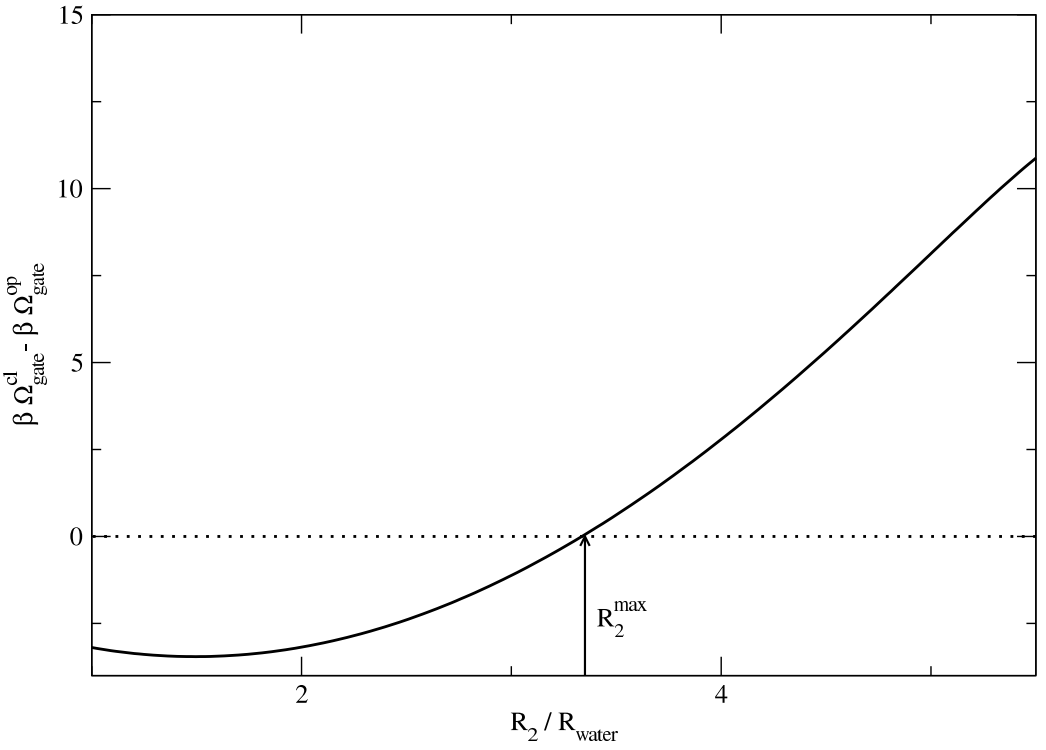

Figure 6.